Understanding the performance of gamma-ray-irradiated epoxy nanocomposites

Palash Mishra[1], Belaguppa Manjunath Ashwin Desai[1], Nilesh Jayantilal Vasa[2], Ramanujam Sarathi[1] ✉, Takahiro Imai[3]

[1]*Department of Electrical Engineering, Indian Institute of Technology Madras, Chennai 600036, India*
[2]*Department of Engineering Design, Indian Institute of Technology Madras, Chennai 600036, India*
[3]*Toshiba Corporation, Power, and Industrial Systems R&D Centre, 1, Toshiba-cho, Fuchu-shi, Tokyo, 183-8511, Japan*
✉ *E-mail: rsarathi@iitm.ac.in*

Epoxy nanocomposites being used in the high-energy radiation zones as an insulant may undergo changes in their dielectric properties during service. In the present study, the performance of base epoxy resin (S1) is compared with epoxy resin with ion trapping particle (Sample S2) and epoxy resin with nanotitania (Sample S3) particle. The influence of gamma irradiation on nanocomposites was analysed. Corona inception voltage due to water droplet initiated discharge and contact angle reduces post-gamma-ray irradiation. Surface potential decay time constant reduced drastically for gamma-ray-irradiated specimens. Trap distribution characterisation indicated that charge mobility increases after irradiation. The surface roughness of the sample increases with the irradiation dosage. Dielectric relaxation spectroscopy shows that permittivity reduces and loss tangent increases with the gamma-irradiated specimens. Water diffusion rate increases for the gamma-ray-irradiated specimen. No change in elemental composition, measured using laser-induced breakdown spectroscopy, of test specimens was observed. The hardness of the material and plasma temperature formed during laser shine decreases with gamma-ray irradiation intensity for Sample S1, whereas samples S2 and S3 showed only marginal variation. The performance of Sample S2 is found to be better than Samples S1 and S3.

1. Introduction: Epoxy resin is one of the most commonly used thermoset material in the power apparatus because of its excellent mechanical, electrical, thermal and chemical stability. It is possible to achieve the desired properties by choosing proper nanofillers. The surface of the nanoparticles is highly active and can enhance the desired properties of the material, even at low concentration of filler [1–4]. Early research works have indicated that the addition of TiO_2 in epoxy resin has improved dielectric properties [5–8]. The study on the effects of addition of inorganic ion exchangers and its impact on the basic dielectric properties of the epoxy resin are scanty. Inorganic ion exchangers have superior ion trapping properties, high heat, and oxidation resistance and thus they can be used in the insulation structure in the power apparatus to improve its reliability [9, 10]. Hence, it is essential to understand the impact of such nanoscale inorganic ion exchangers in the insulating material on its dielectric properties.

Recent times, the polymeric materials are gaining importance to use as insulant in power equipment operated in high-energy radiation zones and are exposed to a different level of irradiation of photons, electron beam, and gamma-ray irradiation. It has been reported that the dose rate in the nuclear power plant varies widely from 10 µGy/h to 10 kGy/h with a total exposure of 1000 kGy [11]. Murray *et al.* [12] studied the impact of polymeric materials to high-energy irradiation and have indicated that radiation can cause material discolouration with increased surface roughness. Due to such characteristic variation, it is necessary to study the impact of this radiation on the dielectric properties and the mechanical properties especially the storage modulus and tan δ of the nanocomposite material.

The water droplets can form on the surface of the insulation structure due to rain or condensation of fog during its operation. It is essential to understand the water diffusion characteristics of the nanocomposite material. In addition, the water droplet formed on the surface of the insulating material can cause field enhancement thereby generating corona followed by surface discharge activity. Sarathi *et al.* have indicated that the water droplet initiated discharges radiates ultra high-frequency (UHF) signal. They have

adopted the UHF technique to identify corona discharge inception. The inception of corona/surface discharges can cause a reduction in hydrophobicity of the material, erosion of material, carbonisation of the surface and finally, the discharge bridges the electrode gap leading to catastrophic failure of the insulation structure [13, 14]. Thus, to understand the impact of high-energy radiation on the insulating material during water droplet-initiated discharges, methodical experimental studies need to be carried out to correlate discharge behaviour with the dosage of gamma radiation. Also, charge accumulation studies can provide characteristic variations in the surface of the material [15]. In recent times, the optical techniques are gaining considerable importance to monitor the condition of the insulating material, during operation. Laser-induced breakdown spectroscopy (LIBS) technique can identify the level of ageing and the composition of insulating material [16].

The present study aims in comparing the performance of virgin and gamma-ray-irradiated specimens of epoxy nanocomposite material, by carrying out the following studies: (i) to understand the surface charge accumulation characteristics of the nanocomposite material; (ii) to analyse the characteristics variation in corona inception voltage (CIV) due to water droplet; (iii) to study the surface characteristics of the irradiated specimens through contact angle and surface roughness of the test specimens; (iv) to compare the dielectric response of the test sample and its dependence on dosage intensity of gamma ray; (v) to evaluate the water diffusion coefficient of irradiated specimens; (vi) to perform the LIBS analysis for determining the change in the emission spectra and plasma temperature of nanocomposite material due to gamma-ray irradiation; and (vii) to analyse the variation in storage modulus and loss factor of the nanocomposite material due to gamma irradiation through dynamic mechanical analysis (DMA) studies.

2. Experimental studies
2.1. Sample preparation: In the present study, the epoxy nanocomposites were characterised. The details of epoxy nanocomposite samples used for this study are listed in Table 1. Standard shearing mixing, degassing, curing procedures were adopted to prepare

Table 1 Sample composition

Sample acronym	Composition, wt%
S1	Base epoxy resin
S2	epoxy resin with the ion trapping particle (hydrocalcite compound modified with zirconium phosphate) (of 2 wt%)
S3	epoxy resin with titania nanoparticle (of 5 wt%)

samples with epoxy as a base matrix [17]. The samples were irradiated by ^{60}Co gamma-rays with a dose rate of 4.5 kGy/h in air medium to total doses of 50 and 100 kGy.

2.2. Experimental setup: The experimental setup used for understanding the water droplet initiated discharge is shown in Fig. 1. The experimental setup can be sectionalised as (i) the high-voltage source, (ii) the test electrode configuration and (iii) the UHF sensor connected to the high bandwidth digital storage oscilloscope to detect corona inception. Details of the experimental setup are described in our previous work [16].

2.3. Surface potential measurement andLIBS: Needle plane configuration was used to spray charges on the composite material, by generating a corona discharge at 12 kV DC.

LIBS is a type of atomic emission spectroscopy which uses a highly energetic laser pulse as the excitation source. LIBS may be used to evaluate the level of each constituent element or to monitor the presence of impurities. In the present study, Nd3+ YAG laser was focused on the sample using 25 cm focal length and guided to the spectrometer (Ocean Optics) through the multimode optical fibre of core diameter 400 μm, 0.22NA is used. Integration period of 1 s was used to get LIBS spectra. Details of the experimental setup for surface potential measurement and LIBS are described in our previous work [16].

2.4. Water diffusion studies: It is essential to understand the diffusion level of water into the insulating material, which alters the resistivity of the material. The test samples were immersed in deionised water and placed in an oven at constant temperature (30°C) and the water absorption with time was measured using the weighing balance with an accuracy of 0.01 mg.

2.5. Dielectric response study: Frequency domain dielectric spectroscopy measurements were carried out to understand the characteristic variation in permittivity and tan δ of the material, at different frequencies. The broadband dielectric/impedance spectrometer (Novo control technology: Alpha-A high-performance frequency analyser) was used to measure the permittivity and tan δ of the epoxy nanocomposite materials, in the frequency range of 1–10^6 Hz at room temperature. The test electrode of 20 mm diameter was used for this study.
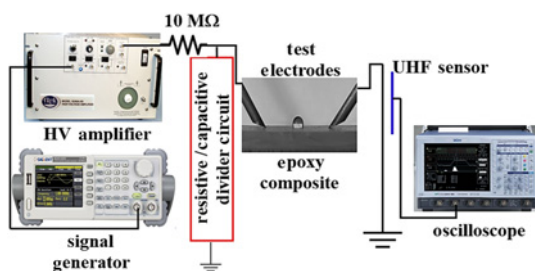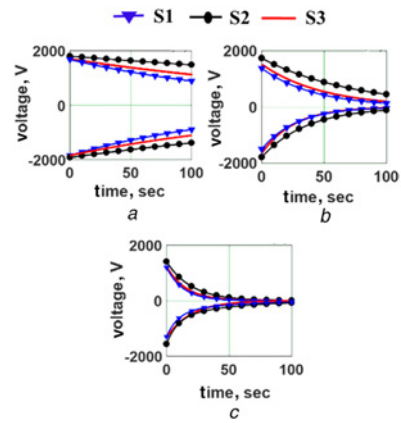

Fig. 1 *Experimental setup*

Fig. 2 *Surface potential decay characteristics for the*
a Virgin
b 50 kGy
c 100 kGy gamma-irradiated specimens

3. Results and discussions

3.1. Surface potential measurement studies: Fig. 2 shows the characteristic variation in surface potential decay characteristic of the virgin and gamma-irradiated specimens of epoxy nanocomposites. It is observed that the surface potential exhibits exponential decay, irrespective of the polarity of the corona charging voltage. Studies have clearly indicated that the surface potential of the insulating material depends upon the polarity of charging voltage, radiation dosage and type of nanofillers or ion trapping particle used as a filler in nanocomposites [18, 19].

Table 2 shows the decay rate of the surface potential of the epoxy nanocomposite attained due to surface charge deposited by corona activity. It is observed that the initial value of surface potential (Fig. 2) and decay time constant (Table 2) is more for the virgin specimens and their values decrease with increase in dosage of gamma-ray irradiation. The cause for such variation could be due to multiple processes such as chain scission, the formation of the polymer radical, cross-linking etc. It is noticed that the test Samples S2 and S3 have less decay rate (Table 2), which is indicative of their superior performance.

Fig. 3 shows the potential distribution over the surface of the virgin and gamma-irradiated specimen after corona charging. A Gaussian-type potential distribution is observed on the surface of the insulating material and it is high near a charging point. It is also observed that the surface potential reduces with increase in gamma irradiation dosage.

Log(t) is proportional to the characteristic time, which is the time at which $td\nu/dt$ curve reaches the peak value and is an indicative of trap depth. $td\nu/dt$ is the indicator to the trap density at the demarcation energy and it is proportional to the detrapping current $I_d(t)$, which generates due to movement of charge carrier near the demarcation energy level E_d into the conduction states. The $I_d(t)$ is proportional to the trap density at the demarcation energy $N(E_d)$ and

Table 2 Initial decay rate of test specimens

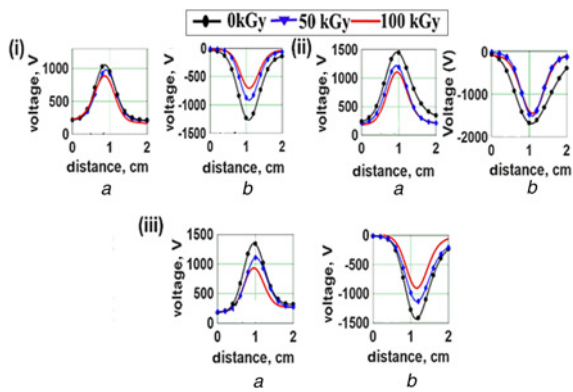| Sample	Decay rate (λ)					
	+DC			−DC		
	0 kGy	50 kGy	100 kGy	0 kGy	50 kGy	100 kGy
S1	0.006	0.023	0.074	0.007	0.036	0.091
S2	0.002	0.014	0.050	0.003	0.028	0.054
S3	0.004	0.020	0.064	0.005	0.034	0.066

Fig. 3 *Potential distribution over the surface of sample (i) S1 (ii) S2 (ii) S3*
a Positive charging
b Negative corona charging

to the rate of change of E_d [20]:

$$I_d(t) \propto \frac{dV}{dt} \propto N(E_d(t)) \frac{dE_d}{dt} \quad (1)$$

$$E_c - E_d = kT \ln(\upsilon t) \quad (2)$$

$$\frac{dV}{dt} \propto N(E_d(t)) \quad (3)$$

where E_c is the conduction band energy level and υ is the attempt to escape frequency. Fig. 4 shows the trap distribution characteristics ($t dv/dt$ versus t) for the virgin and gamma-ray-irradiated specimens. It is observed that the spread of the $t dv/dt$ plot gets reduced with the increase in gamma-ray irradiation dosage from the surface. In general, the left shift in the $t dv/dt$ plot peak for the gamma-irradiated specimens is observed indicating the easy detrapping of charges. This left shift is also the indication of the reduction of the energy barrier for charge detrapping. It is also an indicative that the charges get trapped in the shallow traps in the gamma radiation treated sample in contrast with the virgin sample which has the higher characteristic time and $t dv/dt$ value indicating the presence of more deep traps in it. Further, as clearly visible from Fig. 4, the trapped charge density (indicated by $t dv/dt$) follows the order $S2 > S3 > S1$.

3.2. Variation in contact angle and CIV: The contact angle is an indicative measure of hydrophobicity of the insulating material. Table 3 shows the static contact angle for the virgin and gamma-ray-irradiated specimens. It is observed that the contact
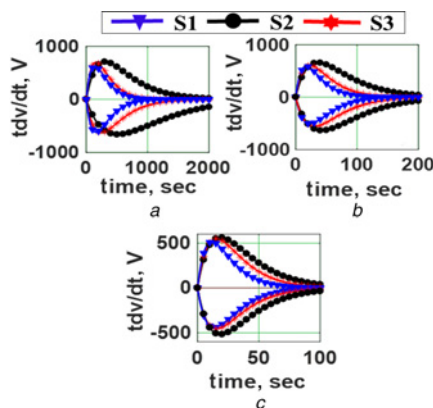
angle decreases with the increase in the radiation dosage. Further, among all the samples, Sample S2 possess the highest contact angle and S1 has the least value.

Fig. 5 shows variation in water droplet-initiated corona discharge inception voltage on epoxy nanocomposites under AC and DC voltages. It is observed that the CIV (calculated using the first UHF signal generated due to water droplet initiated discharges) under AC is much lower than under DC voltage. This could be due to variation in contact angle of the nanocomposite material, conductivity of water droplet, volume of the water droplet, and characteristic change in the shape of the water droplet due to the applied voltage. It is observed that CIV decreases with the increase in radiation dosage possibly due to the reduction in contact angle after gamma-ray irradiation. Table 3 shows the variation in contact angle of the epoxy nanocomposite material with different levels of gamma irradiation. It is observed that the contact angle of the gamma-irradiated specimen shows drastic reduction and is minimum with the S2 specimen. The large variation in contact angle is observed with neat epoxy resin specimen.

The water droplet placed in the electrode gap, on the application of voltage, elongates along the axis of the electrodes. In the process, the water droplet tip gets sharpened and at the triple junction, the local electric field gets enhanced, thereby incepting corona. It is clear from Table 3 and Fig. 5 that the contact angle and CIV follow direct correlation. The decrement in the contact angle indicates that the droplet can spread over the insulating surface thereby reducing the effective distance between the droplet and the electrodes enhancing electric field, thereby the corona formed due to water droplet, to incept at a lower voltage. Thus, overall it is observed that, under AC/DC voltage, the CIV is much higher with S2 specimens than S1 and S3 specimen. This indicates that ion trapping filler allows the material to be radiation resistant.

Fig. 6 shows the variation in decolouration of epoxy nanocomposites due to gamma irradiation. It is clearly observable that the decolouration of the sample takes place due to gamma rays. In order to further investigate the effects of gamma rays over the surface of the test sample, the surface roughness of the specimens was measured

Table 3 Variation in contact angle and surface roughness of gamma-irradiated nanocomposites

Sample	Contact angle			Surface roughness		
	0 kGy	50 kGy	100 kGy	0 kGy	50 kGy	100 kGy
S1	71.3	55.9	48.3	646	691	770
S2	82.3	73.7	65.5	352	401	465
S3	75.1	66.2	51.2	373	453	521

Fig. 4 *Trap distribution characteristics for the*
a Virgin
b 50 kGy
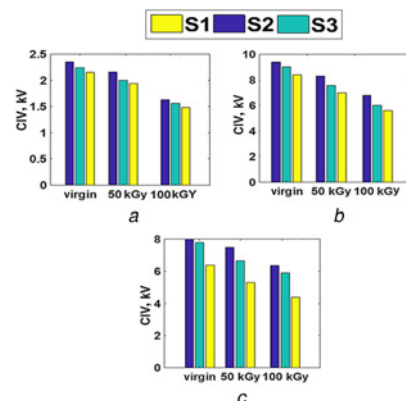*c* 100 kGy gamma-irradiated specimens

Fig. 5 *Variation in CIV for virgin and gamma aged specimen's under*
a AC voltage
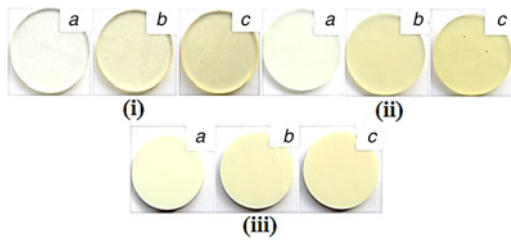*b* Positive DC voltage
c Negative DC voltage

Fig. 6 *Pictorial view of decolouration of sample (i) S1 (ii) S2 (iii) S3 after gamma irradiating at*
a 0 kGy
b 50 kGy
c 100 kGy

using the surface optical profilometer as shown in Table 3. It is observed that the level of surface damage due to irradiation is less with S2 specimen compared to epoxy resin material and S3 specimen.

3.3. Dielectric relaxation spectroscopy: Fig. 7 shows the variation in the permittivity and loss tangent (tan δ) of epoxy nanocomposites with the change in frequency for the virgin and gamma-ray-irradiated specimens. It is observed that the permittivity reduces with the increase in the supply voltage frequency. On increasing the supply voltage frequency, the dipole orientation gets restricted thereby the permittivity reduces. The permittivity of S2 is much higher than S1. Also, it is observed that the permittivity of Sample S2 is highest among all the samples. Comparing the permittivity values of gamma-irradiated specimen, it is observed that the permittivity of gamma-ray-irradiated specimens is less as compared to their virgin specimens. This could be due to the generation of free radicals resulting from the chain scission or oxidation process that occurred due to gamma-irradiated specimen [21].

tan δ values decrease with the frequency and reach a minimum value and above a certain frequency, the tan δ increases with increase in frequency (Fig. 7). Also, for the low-frequency range the tan δ value for S1 is higher than the other test samples but in the high-frequency range beyond 1 kHz, there is no significant difference in the values of tan δ of all the sample.

The dielectric exhibits different polarisations. However, the relaxation of each polarisation process with the increment of frequency nullifies its contribution to the overall polarisation, resulting in a decrement of the permittivity [22]. In the present study, we could obser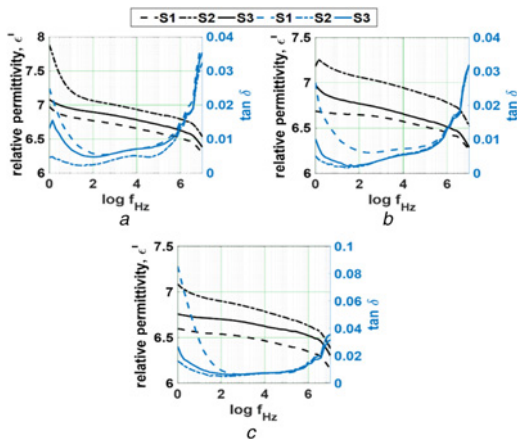ve two relaxations i.e. interfacial/space charge polarisation relaxation and oriental polarisation relaxation. Near the relaxation frequency, the peaking of tan δ is observed. In the frequency range, 1 Hz–1 kHz relaxation of interfacial polarisation and corresponding peaking of tan δ is observed. Interfacial polarisation is due to changes in conductivity which is observed at the boundaries of the matrix and fillers and at the defects in the dielectric. As shown in Fig. 7 at 1 Hz the nanocomposites S2 and S3 exhibit a higher permittivity due to interfacial polarisations basically due to boundary formed by nanofiller and matrix. Similarly, in the range 10^5 Hz–1 MHz orientation polarisation predominates and the corresponding peaking of tan δ is observed [23]. However, in the frequency range, 1 kHz–1 MHz where orientation polarisation is dominant the difference in permittivity amongst the three samples is less compared to the difference in the permittivity at low-frequency range. As the result around 1 MHz when oriental polarisation relaxes, the tan δ shoots up, however difference in the tan δ amongst the three samples is minimum. Also, a marginal increase in the value of the dissipation factor is observed with the gamma-ray-irradiated specimen.

3.4. Water diffusion characteristics: Fig. 8 shows the percentage increase in weight of the specimen due to water ageing. It is observed that the water diffuses into the bulk volume of the specimens and gets saturated after certain time irrespective of radiation dosage. Among three specimens, the intake of water is high with epoxy resin (S1) and minimum with ion trapping particle dispersed epoxy resin (S2).

Water diffusion coefficient is calculated as [24]

$$D = \frac{\pi L_{0.5}^2}{64\, t_{0.5}} \qquad (4)$$

where L is the thickness of the specimen and $t_{0.5}$ is the time of absorption. A reduction in the diffusion coefficient of the material is observed with epoxy nanocomposite material. Since the nanofiller acts as a barrier for diffusion of water into the bulk volume of insulating material. Diffusion level of water increases with an increase in radiation dosage (Table 4). This is due to a reduction in hydrophobicity of the material as radiation caused damage to the insulating material.

3.5. Laser-induced breakdown spectroscopy: Fig. 9 shows the emission spectra of the virgin and gamma-ray-irradiated specimens. It is observed that there is no change in the elemental composition after gamma irradiation for all the samples. However, for Sample S1, the intensity of light emitted by the element reduces with the increase in gamma-ray irradiation intensity as shown in Fig. 9.

Fig. 7 *Variation in real relative permittivity and loss tangent of epoxy nanocomposites after gamma irradiating at*
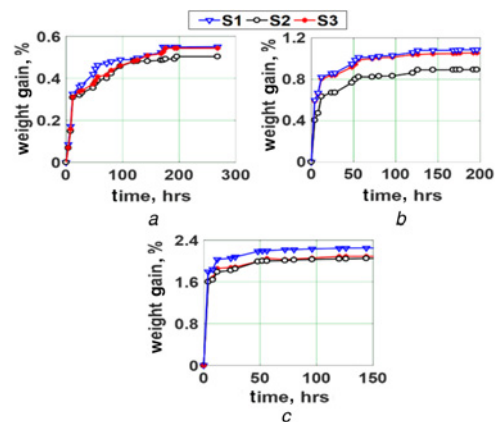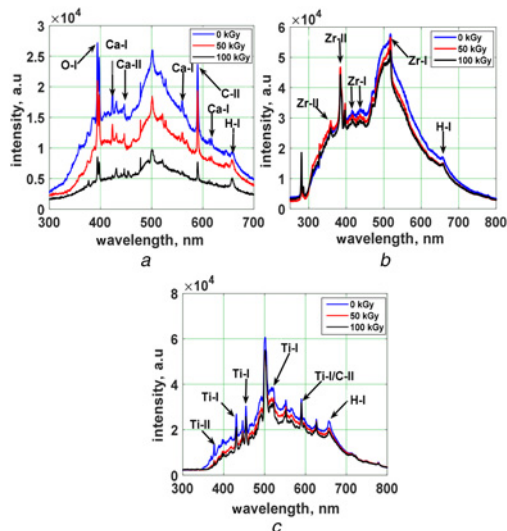*a 0 kGy*
b 50 kGy
c 100 kGy

Fig. 8 *Variation in weight gain in epoxy nanocomposites after gamma irradiating at*
a 0 kGy
b 50 kGy
c 100 kGy

Table 4 Variation in diffusion voefficient with gamma irradiation intensity

Sample	Diffusion coefficient, m²/s × 10⁻¹³			Crater depth, μm		
	0 kGy	50 kGy	100 kGy	0 kGy	50 kGy	100 kGy
S1	3.1694	4.3265	6.8142	389.6	432.6	475.4
S2	2.7813	3.1692	3.7857	276.7	298.7	290.7
S3	3.0974	4.0154	4.5428	331.1	330.4	350.7

Fig. 9 *Emission spectra of the virgin and gamma-ray-irradiated specimens*
a S1
b S2
c S3

Such a behaviour is also seen in other samples but it is negligible to be quantified. Meyer *et al.* [25] have indicated that the amount of laser energy reflected/observed by the specimen depends on the colour of the specimen. A possible reason for the increment in intensity for S1 is the greater absorption of laser light resulting from the sample decolouration as shown in Fig. 6.

Table 5 shows the variation in the plasma temperature which is used to characterise the plasma produced by the ablation of materials through the interaction of the laser beam on the surface of the samples. The plasma temperature is calculated using the Boltzmann–Saha equation:
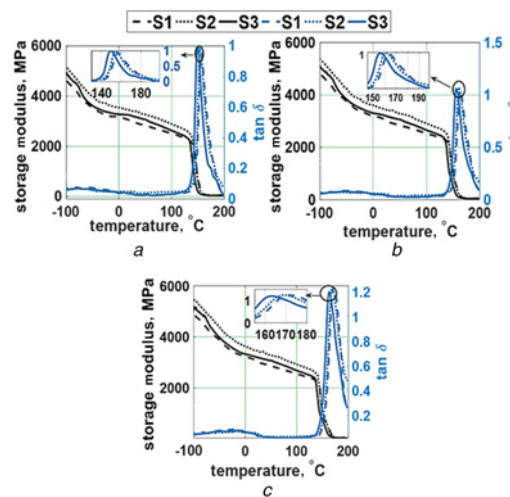
$$T_e = 1.44 \frac{E_2 - E_1}{\ln\left[(l_1 \lambda_1 A_2 g_2)/(l_2 \lambda_2 A_1 g_1)\right]} \quad (5)$$

where E_1 and E_2 are excited energy levels, g_1 and g_2 are statistical weights of excited energy levels 1 and 2, respectively, A_1 and A_2 are transition probabilities of states, I_1 and I_2 are intensities of particular atomic species at λ_1 and λ_2 wavelength, respectively, and T_e is the plasma electron temperature under the condition of local thermodynamic equilibrium.

It is observed that plasma temperature and Vickers hardness (Table 5) follows the order 100 kGy < 50 kGy < 0 kGy for Sample S1 but the other samples show negligible variation in plasma temperature and Vickers hardness. In several studies, it is stated that plasma temperature is directly proportional to the hardness of the material [26]. In the present study also hardness varies as 100 kGy < 50 kGy < 0 kGy for Sample S1. The reason for such behaviour is that irradiation can possibly result in cross-linking/degradation reaction. These clearly indicate that the gamma-ray irradiation has resulted in degradation reaction in Sample S1 while in the other samples (S2, S3) the effect is negligible in terms of mechanical hardness and plasma temperature hence it

Table 5 Variation in plasma temperature and Vicker hardness

Sample	Plasma temperature, K			Vicker hardness (HV0.5/15)		
	0 kGy	50 kGy	100 kGy	0 kGy	50 kGy	100 kGy
S1 (Ca)	7890	7056	6290	16.3	14.7	11.3
S2 (Zr)	9621	9605	9583	23.7	23.2	22.3
S3 (Ti)	8340	8263	8390	20.2	19.9	20.9

Fig. 10 *Variation in storage modulus and damping factor (tan δ) for epoxy/epoxy nanocomposites a function of temperature under*
a 1 Hz
b 10 Hz
c 50 Hz sinusoidal mechanical

Table 6 Variation in glass transition temperature

Sample	Glass transition temperature, °C			Activation energy, kcal/mol
	1 Hz	10 Hz	50 Hz	
S1	156.2	163.7	171.2	99.6
S2	153.5	161.0	168.5	104.0
S3	149.7	155.7	162.7	104.6

can be concluded that nanofiller is prohibiting either cross-linking/degradation reaction resulting by irradiation.

3.6. Dynamic mechanical analysis: Fig. 10 shows the variation in the storage modulus and tan δ for the base epoxy resin/epoxy nanocomposite. As a general trend, it is observed that the storage modulus reduces with the increase in temperature and decreases in frequency. Glass transition temperature and activation energy for all the test samples were calculated from the peak of the tan δ curve (Table 6). It is observed that the inclusion of nanoparticle increases the activation energy and decreases the glass transition

temperature. The cause for it could be due to reduction in crosslinking process in the material due to inclusion of nano particles.

In the glassy region, storage modulus of nanocomposites is higher than pure epoxy, however in the rubbery region the storage modulus for all the three samples is nearly the same. Further, T_g (glass transition temperature) is lower for nanocomposites compared to pure sample. Therefore, the increased storage modulus in the glassy region can be attributed to the nanofiller addition with higher elastic modulus compared to the epoxy. Addition of nanoparticles can have two effects – reduced cross-linking density and immobilisation of polymer chain due to reduced interparticle distance. Immobilisation would reduce storage modulus and increase T_g. However, we have observed reduced T_g and increased storage modulus (Table 6). Increased storage modulus is attributed to nanofiller addition with higher elastic modulus and reduced T_g is due to decreased cross-linking. Also, nanocomposites have higher activation energy compared to pure epoxy (Table 6). The maximum enhancement of storage modulus is found in Sample S2 filled with zirconium ion trapping particle.

4. Conclusions: Dielectric behaviour of the virgin and gamma-ray-irradiated epoxy nanocomposites were investigated in the present study. The important conclusions accrued based on the study are as follows:

• Surface charge accumulation studies have shown that a reduction in decay time constant and a decrease in surface charge magnitude for the gamma-ray-irradiated specimens. A left shift in the trap distribution characteristics is observed with the gamma-irradiated specimen, indicating a decrement in the demarcation energy level. The contact angle has decreased with an increase in surface roughness as observed for the gamma-irradiated specimen.

• Water droplet studies revealed that the CIV reduces with the gamma-irradiated specimen. This confirms that CIV due to water droplet and its contact angle follows a direct correlation.

• Epoxy reinforced with nanofillers exhibited a marginal increase in permittivity of the material as evident from the present study. Also, gamma-irradiated specimen depicts a marginal reduction in permittivity of the material. At low frequency, the tan δ decreases up to certain frequency and above which it increases. The tan δ increases for the gamma-irradiated specimen. It is also observed that the conductivity and frequency follow almost the linear relationship.

• LIBS studies have shown no change in the elemental composition of the material with gamma-ray-irradiated specimen compared with virgin material. However, marginal decrement in the emission spectra intensity of Sample S1 is observed. A direct linear relationship is observed between plasma temperature and hardness of the material and its value decreases with an increase in the level of gamma-ray irradiation intensity.

• Nanofillers exerted a high impact on reduction in water diffusion to epoxy nanocomposite material. However, with the increase in the gamma-ray irradiation intensity, the rate of water diffusion increases.

• DMA analysis has shown that the incorporation of the nanofillers leads to a decrease in the glass transition temperature. Also, the increase in the activation energy of base epoxy resin is observed after the inclusion of nanofillers.

5 References

[1] Iyer G., Gorur R.S., Richert R., ET AL.: 'Dielectric properties of epoxy based nanocomposites for high voltage insulation', *IEEE Trans. Dielectr. Electr. Insul.*, 2011, **18**, (3), pp. 659–666

[2] Imai T., Sawa F., Nakano T., ET AL.: 'Effects of nano and micro-filler mixture on electrical insulation properties of epoxy based composites', *IEEE Trans. Dielectr. Electr. Insul.*, 2006, **13**, (1), pp. 319–326

[3] Cao Y., Irwin P.C., Younsi K.: 'The future of nanodielectrics in the electrical power industry', *IEEE Trans. Dielectr. Electr. Insul.*, 2004, **11**, (5), pp. 797–807

[4] Singha S., Thomas M.J.: 'Dielectric properties of epoxy nanocomposites', *IEEE Trans. Dielectr. Electr. Insul.*, 2008, **15**, (1), pp. 373–385

[5] Yong-Hong C., Zeng-Bin W., KaiStudy W.: 'Pulsed vacuum surface flashover characteristics of epoxy composites with micro TiO_2 and $Al_2O_3.3H_2O$ filler', *IEEE Trans. Plasma Sci.*, 2012, **40**, (1), pp. 68–77

[6] Nelson J.K., Hu Y., Thiticharoenpong J.: 'Electrical properties of TiO_2 nanocomposites'. IEEE Conf. Electrical Insulation Dielectric Phenomena (CEIDP), Albuquerque, NM, USA, 2003, pp. 719–722

[7] Katayama J., Ohki Y., Fuse N., ET AL.: 'Effects of nanofiller materials on the dielectric properties of epoxy nanocomposites', *IEEE Trans. Dielectr. Electr. Insul.*, 2013, **20**, (1), pp. 157–165

[8] Singha S., Thomas M.J.: 'Permittivity and tan delta characteristics of epoxy nanocomposites', *IEEE Trans. Dielectr. Electr. Insul.*, 2008, **15**, (1), pp. 2–11

[9] Kraus K.A., Phillips H.O.: 'Adsorption on inorganic materials I. Cation exchange properties of zirconium phosphate', *J. Am. Chem. Soc.*, 1956, **78**, (3), pp. 694–694

[10] Amphlett C., McDonald L., Redman M.: 'Synthetic inorganic ion-exchange materials-I zirconium phosphate', *J. Inorg. Nucl. Chem.*, 1958, **6**, (3), pp. 220–235

[11] Kyoto M., Chigusa Y., Ohe M., ET AL.: 'Gamma-ray radiation hardened properties of pure silica core single-mode fiber and its data link system in radioactive environments', *J. Lightwave Technol.*, 1992, **10**, (3), pp. 289–294

[12] Murray K.A., Kennedy J.E., McEvoy B., ET AL.: 'Effects of gamma ray and electron beam irradiation on the mechanical, thermal, structural and physicochemical properties of poly (ether-block-amide) thermoplastic elastomers', *J. Mech. Behav. Biomed. Mater.*, 2012, **81**, pp. 252–268

[13] Sarathi R., Sri Harsha V., Griffiths H., ET AL.: 'Understanding water droplet initiated discharges on epoxy nanocomposites under harmonic AC voltages adopting UHF technique', *IEEE Trans. Dielectr. Electr. Insul.*, 2014, **21**, (2), pp. 918–925

[14] Sarathi R., Mishra P., Gautam R., ET AL.: 'Understanding water droplet initiated discharges on damage caused to corona aged silicone rubber', *IEEE Trans. Dielectr. Electr. Insul.*, 2017, **24**, (4), pp. 2421–2431

[15] Kumara S., Serdyuk Y.V., Gubanski S.M.: 'Surface charge decay on polymeric materials under different neutralization model in air', *IEEE Trans. Dielectr. Electr. Insul.*, 2011, **18**, (5), pp. 1779–1788

[16] Ashwin Desai B.M., Mishra P., Vasa N.J., ET AL.: 'Understanding the performance of corona aged epoxy nano micro composites', *Micro & Nano Letters*, 2018, **13**, (9), pp. 1280–1285, doi: 10.1049/mnl.2018.0164, Online ISSN 1750-0443

[17] Imai T., Sawa F., Ozaki T., ET AL.: 'Evaluation of insulation properties of epoxy resin with nano-scale silica particles'. Proc. Int. Symp. on Electrical Insulating Materials (ISEIM), Kitakyushu, Japan, 2005, No. A4-5, pp. 239–242

[18] Gao Y., Du B.X., Ma Z.L., ET AL.: 'Decay behavior of surface charge on gamma-ray irradiated epoxy resin'. Proc. IEEE Int. Conf. Solid Dielectrics (ICSD), Potsdam, Germany, 2010, pp. 1–4

[19] Du B.X., Zhang J.W., Gao Y.: 'Effects of TiO_2 particles on surface charge of epoxy nanocomposites', *IEEE Trans. Dielectr. Electr. Insul.*, 2012, **19**, (3), pp. 755–762

[20] Molinié P.: 'Measuring and modeling transient insulator response to charging: the contribution of surface potential studies', *IEEE Trans. Dielectr. Electr. Insul.*, 2005, **12**, (5), pp. 939–950

[21] Laghari J.R., Hammoud A.N.: 'A brief survey of radiation effects on polymer dielectrics', *IEEE Trans. Nucl. Sci.*, 1990, **37**, (2), pp. 1076–1083

[22] Gorur G.R.: 'Dielectrics in electric fields' (CRC Press Taylor and Francis Group, Boca Raton, FL, 2016), pp. 137–141

[23] Johnscher A.K.: 'Dielectric relaxation in solids' (Chelsea Dielectrics Press, London, UK, 1983)

[24] Crank J.: 'Mathematics of diffusion' (Oxford Science Publications, New York, NY, 1975, 2nd edn.)

[25] Meyer L.H., Jayaram S., Cherney E.A.: 'A novel technique to evaluate the erosion resistance of silicone rubber composites for high voltage outdoor insulation using infrared laser erosion', *IEEE Trans. Dielectr. Electr. Insul.*, 2005, **12**, (6), pp. 1201–1208

[26] Cowpe J.S., Moorehead R.D., Moser D., ET AL.: 'Hardness determination of bio-ceramics using laser-induced breakdown spectroscopy', *Spectrochim. Acta B*, 2011, **66**, (3–4), pp. 290–294